Received: 7 November 2017 | Accepted: 10 April 2018

DOI: 10.1002/hyp.11628

RESEARCH ARTICLE

WILEY

Spatio-temporal tracer variability in the glacier melt end-member — How does it affect hydrograph separation results?

Jan Schmieder[1] | Jakob Garvelmann[2] | Thomas Marke[1] | Ulrich Strasser[1]

[1] Department of Geography, University of Innsbruck, 6020 Innsbruck, Austria

[2] Institute of Meteorology and Climate Research—Atmospheric Environmental Research, Karlsruhe Institute of Technology, 82467 Garmisch-Partenkirchen, Germany

Correspondence
Jan Schmieder, Department of Geography, University of Innsbruck, 6020 Innsbruck, Austria.
Email: jan.schmieder@uibk.ac.at

Funding information
Austrian Academy of Sciences

Abstract

Geochemical and isotopic tracers were often used in mixing models to estimate glacier melt contributions to streamflow, whereas the spatio-temporal variability in the glacier melt tracer signature and its influence on tracer-based hydrograph separation results received less attention. We present novel tracer data from a high-elevation catchment (17 km^2, glacierized area: 34%) in the Oetztal Alps (Austria) and investigated the spatial, as well as the subdaily to monthly tracer variability of supraglacial meltwater and the temporal tracer variability of winter baseflow to infer groundwater dynamics. The streamflow tracer variability during winter baseflow conditions was small, and the glacier melt tracer variation was higher, especially at the end of the ablation period. We applied a three-component mixing model with electrical conductivity and oxygen-18. Hydrograph separation (groundwater, glacier melt, and rain) was performed for 6 single glacier melt-induced days (i.e., 6 events) during the ablation period 2016 (July to September). Median fractions (±uncertainty) of groundwater, glacier melt, and rain for the events were estimated at 49±2%, 35±11%, and 16±11%, respectively. Minimum and maximum glacier melt fractions at the subdaily scale ranged between 2±5% and 76±11%, respectively. A sensitivity analysis showed that the intraseasonal glacier melt tracer variability had a marked effect on the estimated glacier melt contribution during events with large glacier melt fractions of streamflow. Intra-daily and spatial variation of the glacier melt tracer signature played a negligible role in applying the mixing model. The results of this study (a) show the necessity to apply a multiple sampling approach in order to characterize the glacier melt end-member and (b) reveal the importance of groundwater and rainfall–runoff dynamics in catchments with a glacial flow regime.

KEYWORDS

glacier melt, high-elevation catchment, mountain hydrology, streamflow components, tracer variability, tracer-based mixing model

1 | INTRODUCTION

Large parts of the world are highly dependent on glacial meltwater contribution (originating from ice, snow, firn, and temporally stored rain) to streamflow (Barnett, Adam, & Lettenmaier, 2005; Kaser, Großhauser, & Marzeion, 2010; Lemke et al., 2007), especially during dry periods (Frenierre & Mark, 2014). Glaciers are important water reservoirs, which have a compensation effect (Lang, 1986). A

consistent reduction of global ice mass (IPCC, 2013) may threaten future water usage in a variety of regions and climates. Meltwater originating from glaciers can be seen as a nonrenewable water resource under the scope of negative glacier mass balances (Immerzeel & Bierkens, 2012), and accurate assessment of its contribution to basin wide runoff is mandatory for climate change related sustainable water resources management in glacierized watersheds (Miller, Immerzeel, & Rees, 2012; Schaner, Voisin, Nijssen, & Lettenmaier, 2012; Viviroli et al., 2011). In the European Alps, stream water is often used for irrigation and hydro power generation (Beniston, 2012; Schaefli, Hingray, & Musy, 2007), as well as for snow making (Rixen et al., 2011). Because mountain streams are composed of water originating from glaciers, snow, rain, and subsurface storages (Cable, Ogle, & Williams, 2011; Moser & Stichler, 1980; Yde et al., 2016), it is crucial to assess the quantification of streamflow components, to investigate the origin of water, and to improve the understanding of streamflow generation in glacierized catchments under the scope of a changing climate.

Among different and often used methods to quantify the contribution of glacial meltwater to streamflow (i.e., hydrological modelling, direct discharge measurements, hydrological balance equations, and glaciological approaches), the tracer-based approach requires the smallest amount of data (Frenierre & Mark, 2014) and has relative rarely been used in glacierized environments. By simple mass balances of tracer concentrations in the stream and in the end-members that are forming discharge, the fraction can be determined. The assumption that end-member tracer signatures need to be unique is fundamental for applying this approach but is often given due to different water origins as a result of hydrological processes in a catchment (Drever, 1997). Tracers applied within this method should be conservative, that is, no change in signature (e.g. due to isotopic fractionation or chemical reaction of solutes with geology) except due to mixing of different waters (Baraer, McKenzie, Mark, Bury, & Knox, 2009; Mark, McKenzie, & Gómez, 2005). Environmental tracers, such as electrical conductivity (EC), and stable isotopes of water, such as oxygen-18 ($\delta^{18}O$), have been used in tracer-based hydrologic studies of glacierized catchments (e.g., Engel et al., 2016; Rodriguez, Ohlanders, Pellicciotti, Williams, & McPhee, 2016; Williams, Wilson, Tshering, Thapa, & Kayastha, 2016). The spatio-temporal variability in end-members violates the assumption of uniqueness and can be a limiting factor in applying mixing models. The end-member tracer signature variability is crucial for applying mixing models and therefore should be addressed in future studies as Penna, Engel, Bertoldi, and Comiti (2017) and Frenierre and Mark (2014) pointed out. As an example, Penna et al. (2017) advise to define end-member tracer signature dynamically and call for temporal sampling at high frequencies, which was rarely done for the glacier melt or groundwater end-member. Klaus and McDonnell (2013) highlighted the importance of spatial variability in end-member tracer signatures in their review on isotopic hydrograph separation, which should be investigated in future studies. This was also rarely done for the glacier melt and the groundwater end-member in high-elevation catchments. The spatio-temporal variation in end-member tracer signatures is difficult to characterize at the catchment scale (Hoeg, Uhlenbrook, & Leibundgut, 2000), in particular for glacierized catchments (Jeelani, Shah, Jacob, & Deshpande, 2017), and is affecting mixing model results and uncertainty estimates (Penna et al., 2017). In some studies, a limited number of samples (up to 3) was used to characterize the glacier melt end-member (e.g., Kong & Pang, 2012; Liu et al., 2008; Nolin, Phillippe, Jefferson, & Lewis, 2010), whereas Maurya et al. (2011) used the average value of 20 samples. Using either a few temporally distributed samples or one average value per melt season value cannot capture the natural spatio-temporal variability and hence potentially leads to an under- or overestimation of the glacier melt fraction and high uncertainties. Recent studies have used a time-variant definition of end-members at the monthly scale (Penna et al., 2017; Wu et al., 2016), whereas others used seasonal average tracer signatures (Liu, Han, Chen, Lin, & Wang, 2016; Maurya et al., 2011). Penna et al. (2017) pointed out the need for investigating the intra- and interannual tracer signature variability of glacier melt.

Meltwater can frequently represent a high proportion (>50%) of bankfull discharge (Penna et al., 2017). Recent studies estimated glacier melt contributions with tracer-based mixing models in different mountainous regions worldwide up to 70–80% (e.g., Cable et al., 2011; Kong & Pang, 2012;Penna et al., 2017; Williams et al., 2016). Rainfall contributions to streamflow have often been investigated in temperate humid catchments (Klaus & McDonnell, 2013), but research on rainfall–runoff dynamics in glacierized catchments is rare. Despite melt dominance in those catchments (snow and ice), episodic rainfall events can contribute to streamflow notably (Dahlke, Lyon, Jansson, Karlin, & Rosqvist, 2014). Dahlke et al. (2014) estimated rainfall contributions to streamflow in a 30% glacierized catchment (21.7 km^2) in Sweden at the event scale by up to 58% during the ablation period in 2011. There exists scarce information on the role of groundwater in glacierized high-elevation catchments, and Frenierre and Mark (2014) emphasize to investigate the nexus between dynamics of groundwater and glacier melt contribution to streamflow. Recent studies estimated groundwater fractions at up to 80% in different mountainous regions with contrasting climates at the event scale (e.g., Baraer et al., 2009; Engel et al., 2016; Wilson, Williams, Kayastha, & Racoviteanu, 2016).

The variability in the tracer signature of glacier melt is a large source of uncertainty in estimating glacier melt fractions of streamflow (Cable et al., 2011) but important for applying tracer-based hydrograph separation. Here, we quantify its impact on three-component hydrograph separation results and draw implications for further research. The overall scientific objective is to evaluate dynamics of rain, groundwater, and glacier melt contribution to streamflow during melt-induced events in a high-elevation catchment. This study specifically aims (a) to quantify the tracer variability ($\delta^{18}O$, EC) of the end-members groundwater (i.e., winter baseflow) and glacier melt at the subdaily to monthly scale, as well as at the local scale (only for glacier melt; spatial extent <1,400 m); (b) to estimate streamflow fractions and associated uncertainties by tracer-based hydrograph separation; and (c) to identify the sensitivity of the hydrograph separation results to the natural spatio-temporal variability of the glacier melt end-member.

2 | STUDY AREA

The study was conducted in the Hochjochbach catchment, a subbasin of the Rofenache catchment, which is a long-term Alpine research site

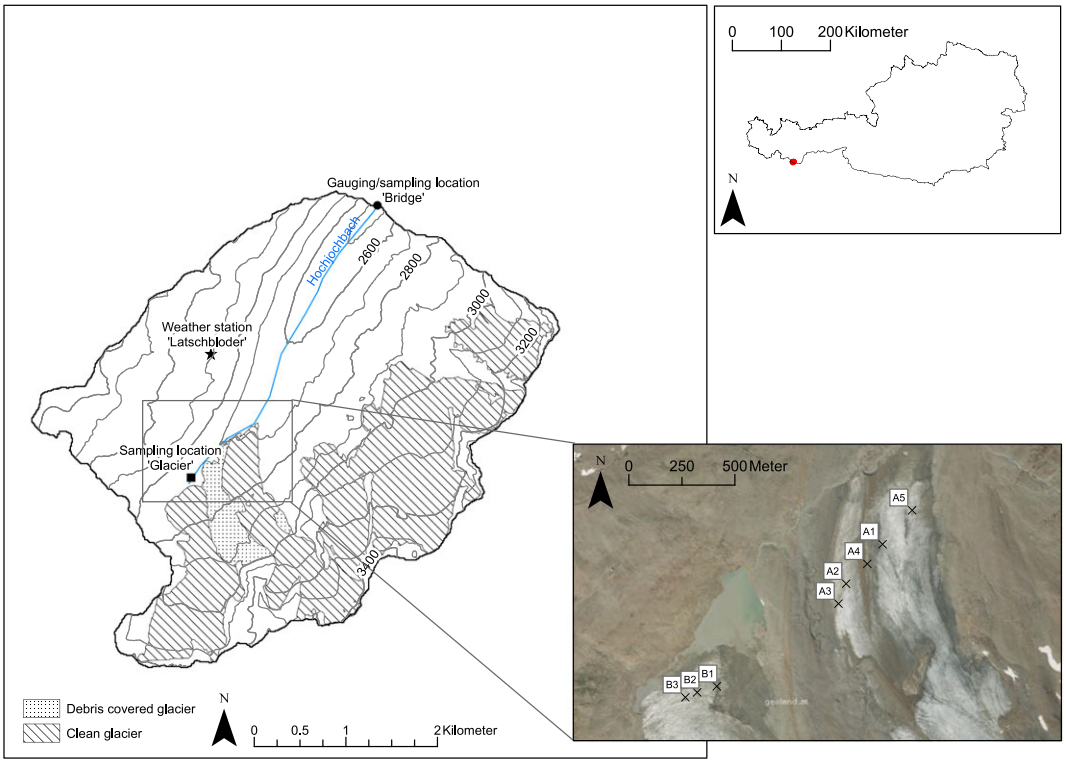

FIGURE 1 Hochjochbach catchment and sampling locations. Inlays show the location of the study area in Austria (upper right panel) and the glacier melt sampling locations on both tongues of the Hochjochferner (lower right panel; data source orthophoto: www.geoland.at, 2016)

with a comprehensive data set of meteorological, hydrological, and glaciological observations (Strasser et al., 2018). The 17.1 km^2 high-elevation catchment (Figure 1) is located in the Austrian Alps (N46°46′–N46°49′/E10°47′–E10°51′), is drained by the Hochjochbach stream, which is trending from southwest to northeast (gauging station at 2,450 m a.s.l.), and ranges up to 3,520 m a.s.l. (mean altitude: 2,950 m a.s.l.). The mean slope of the catchment is 21°. Two glaciers (Hochjochferner and Kreuzferner) cover an area of 34%. Mean length change recorded for Hochjochferner is −27 m/year for the period 2007 to 2016 (WGMS, 2017). Mass balance for the Hochjochferner was estimated (glaciological method) at −244 kg/m^2 for the year of 2013/2014 with an Equilibrium-Line Altitude of 3,055 m a.s.l. (Prantl et al., 2017). Two tongues of the Hochjochferner are connected with a debris-covered part, and their glacier outlet flow directly enters the Hochjochbach stream (cf. Figure 1). The remaining area of the catchment is covered by bedrock outcrops and unconsolidated bare rocks (61%), as well as by sparsely vegetated area (5%, alpine meadows; CLC, 2012). The unconsolidated bare rock area is characterized by glacial deposit (moraine, till), alluvium, alluvial fans, and talus material. The geology consists of paragneiss and mica schist and is overlain by a mantle of glacial deposits and soils (<1 m depth). Mean annual temperature and precipitation at the automatic weather station "Latschbloder" (2,920 m a.s.l.) during the water year 2016 (October to September) were −1.66 °C and 1,125 mm (54% as snow, when air temperature <0 °C), respectively. Runoff at the gauging station "Bridge" during the water year 2016 was 1,619 mm and is seasonally influenced by snow and glacier melt, clearly indicating a glacial flow regime. Approximately 65% of annual runoff concentrated between July and September.

3 | METHODS

3.1 | Event characterization

Six events (#1 to #6) were defined as single glacier melt-induced days during the ablation period (July to September) when most of the snow has disappeared in the catchment (in mid-July, there was a patchy snow cover above 3,000 m a.s.l. at north-facing slopes that ceased towards early August). The events were characterized by mean daily temperatures >1 °C at 2,920 m a.s.l., distinct diurnal variation in streamflow (CV > 0.3, except for event #6), low precipitation amounts (<4 mm; rainfall only observed for events #2 and #4), clear sky (during most of the day), and less or equal than 2 mm rain observed 24 hr prior to the event (cf. Figure 2b–g). The winter baseflow period (December to March) was characterized by low air temperatures and low variability in discharge, when snowmelt, glacier melt, and rain contribution to streamflow is negligible and streamflow is assumed to be supplied by groundwater only.

3.2 | Hydro-climatologic measurements, sampling design, and tracer analyses

Discharge (hourly values) was measured at the gauging station "Bridge" (at 2,450 m a.s.l., cf. Figure 1). The air temperature and precipitation (hourly values) were measured at an automatic weather station (Marke & Strasser, 2017), namely, "Latschbloder" (at 2,920 m a.s.l., cf. Figure 1). We calculated the antecedent precipitation index (API) for 1- to 7-day periods to capture a wide range of moisture conditions and to relate it to the rainfall fraction in streamflow. In the next step, we chose API$_2$

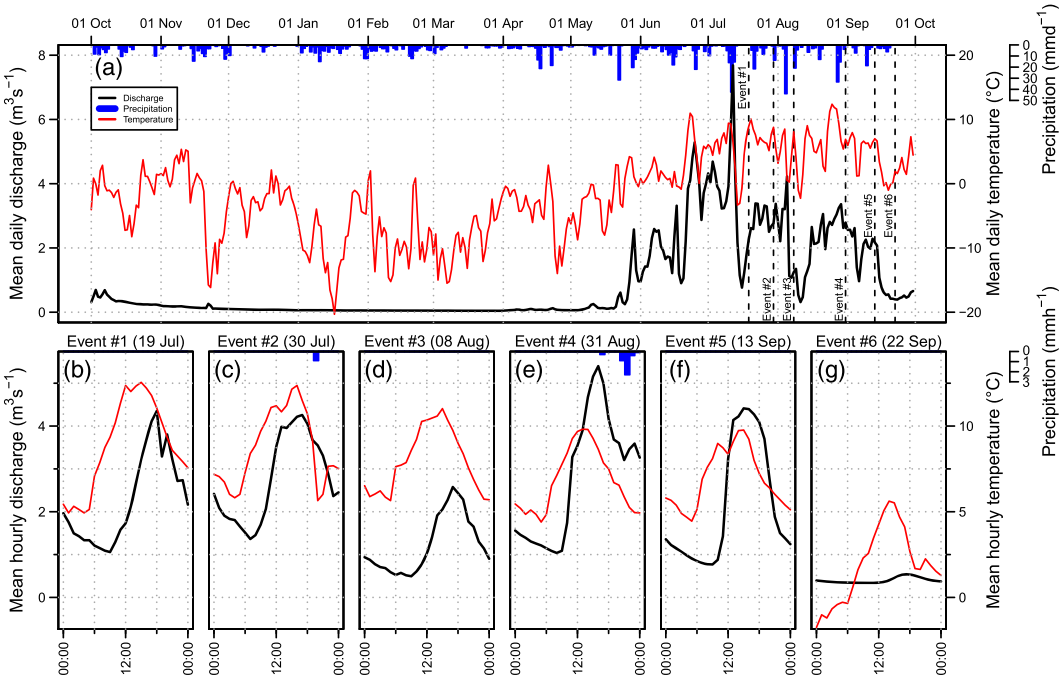

FIGURE 2 Hydro-climatological conditions during the water year 2016 (a) and during the investigated events (b–g)

and API_7 for further analyses (for correlation analyses, see Section 4.3) to capture various wetness conditions for each of the events and to make sure that every event receives a remarkable amount of rainfall (i.e., an arbitrary threshold of 19 mm). Furthermore, the selection of API_2 and API_7 allows for a comparison between conditions that occurred close and not-so-close to an event.

Streamflow was sampled manually (grab samples) at the gauging station "Bridge" (n = 19 in total) during the events. Two to five samples between 09:00 and 16:00 (CET) were collected at 1- to 5-hourly intervals per event. Winter baseflow samples (n = 14) were collected at the same location on December 22, 2015, January 28, and March 17, 2016. The samples of March 17, 2016 (nine out of 14) were collected at a 30-min interval between 11:30 and 15:30 (CET) to identify the potential subdaily variability in the tracer signature. Supraglacial meltwater (n = 51 in total) was sampled approximately every 100 to 200 m along a contour line parallel transect (A1 to A5, see inlay in Figure 1) on the ablation area during four field days (events #1 to #4) at approximately 12:30 (CET) to investigate the spatial and the intraseasonal variability of glacier melt. During two events (#5 and #6), supraglacial meltwater was sampled approximately every 50 to 250 m along contour line parallel transects (two transects per sampling day with three samples per transect, A1 to A3, B1 to B3) at 10:00, 13:00, and 15:30 (CET) to include a potential subdaily variability and a larger spatial range (cf. Figure 1). Rain (n = 9 in total) was sampled by collectors at two sites ("Bridge" and "Glacier," cf. Figure 1) during the study period when liquid-phase precipitation occurred and represents bulk values. The polyethylene collectors (Ø: 10 cm) were filled with a 0.5 cm mineral oil layer to prevent evaporation and were installed at 1.20 m above the surface. Rain samples were recovered on June 23, 2016 and during each of the events (for dates, please see Figure 1).

EC was measured with a portable probe (WTW ProfiLine Cond 3310) with temperature compensation (25 °C) in situ. The measurement precision is 0.1 µS/cm. Water samples collected in the field were stored in dark and cold in high-density polyethylene bottles until analyses for $\delta^{18}O$ with cavity ring-down spectroscopy (Picarro L1102-i) in the laboratory. The measurement precision is 0.1‰.

3.3 | Hydrograph separation and uncertainty analyses

Hydrograph partitioning with environmental tracers is based on mass balances of water (Equation (1)) and tracers (Pinder & Jones, 1969). A two-tracer, three-component mixing model (Ogunkoya & Jenkins, 1993) was applied to partition the streamflow (Q_t) into the groundwater (Q_g), rain (Q_r), and glacier melt component (Q_m). A successful separation of streamflow requires that (a) tracer signatures of water sources differ significantly; (b) contributing water sources maintain constant tracer signatures or their variability can be quantified; (c) streamflow is composed solely of those three components; (d) tracers mix conservatively (a comprehensive description of model assumptions can be found in Buttle, 1994; Hinton, Schiff, & English, 1994; Klaus & McDonnell, 2013; Rodhe, 1987).

$$Q_t = Q_g + Q_r + Q_m, \tag{1}$$

$$Q_t C_t = Q_g C_g + Q_r C_r + Q_m C_m, \tag{2}$$

$$Q_t \delta_t = Q_g \delta_g + Q_r \delta_r + Q_m \delta_m. \tag{3}$$

Equations (2) and (3) show the resulting mass balances of water and tracer fluxes. Input for Equation (2) are EC values of total streamflow (C_t) and the conceptual water sources (end-members)

groundwater (C_g), rain (C_r), and glacier melt (C_m). δ_t, δ_g, δ_r, and δ_m represent the $\delta^{18}O$ composition of total streamflow, groundwater, rain, and melt for Equation (3), respectively. Winter baseflow was assumed to reflect and integrate the hydrochemistry of (shallow) groundwater, as used in other studies (e.g., Fischer, Stähli, & Seibert, 2016; Klaus & McDonnell, 2013; Penna et al., 2017; Sklash, 1990). Hence, the groundwater end-member is characterized by the mean tracer signature of winter baseflow. The rain end-member was characterized by the rain samples. For the days where two bulk samples could be obtained, they were volume-weighted with rain depths to incorporate the spatial variability. To account for the temporal variability and slower flow paths of rain routing through the subsurface, the incremental mean intensity method after McDonnell, Bonell, Stewart, and Pearce (1990) was applied for the mixing model. The glacier melt end-member is characterized by the tracer signature of supraglacial meltwater samples and can constitute of ice melt, firn melt, snowmelt, and temporally stored rain. Because glacier melt sampling was conducted mainly during rain-, snowmelt- and firn melt-free periods, we assume ice melt to be the dominant component. In order to reveal the effect of the varying glacier melt tracer signature on the estimated glacier melt fraction, we performed a sensitivity analysis and characterized the glacier melt end-member temporally variable at the event scale (Approach A), seasonally time-invariant (Approach B), temporally variable at the subdaily scale (Approach C, subdaily data were only for events #5 and #6 available), and also spatially variable in Approach D (Table 1). A time-invariant baseflow tracer signature and a time-variant rain end-member characterization were used for all approaches (as described above). We assumed a negligible snowmelt contribution to streamflow, except that originating from the glacier surface. During field work in July, this assumption was visually ensured as the winter snowpack has almost disappeared on bare ground (cf. Section 3.1). Intermittent snowfall events were assumed to have a small snow water equivalent and negligible influence on the analyses.

For the uncertainty analysis, the Gaussian error propagation method (Genereux, 1998) with a confidence level of 95% was applied. Factors including the spatio-temporal variability of the end-members and the laboratory uncertainty were taken into account. The spatio-temporal variability was accounted for by using the standard deviation of tracer signatures in the samples collected at different locations over time. According to the device manuals (measurement precision), 0.1 μS/cm and 0.1‰ were used as the laboratory uncertainty in the analyses for EC and $\delta^{18}O$, respectively.

4 | RESULTS

4.1 | Hydro-climatological conditions

The winter baseflow period (December to March, Figure 2a) was characterized by an average discharge of 0.06 m^3/s and a small variation in discharge (CV = 0.24). The average air temperature was −7.1 °C, and the observed precipitation sum (approximately 95% as solid phase) was 268 mm during this period (Table 2). The six investigated events

TABLE 1 End-member characterization for the mixing model approaches (A–D)

Approach	Description of glacier melt end-member tracer variability	Glacier melt end-member	Rain end-member	Groundwater end-member
A	Time-variant at subseasonal scale	Average EC and $\delta^{18}O$ of supraglacial meltwater samples taken during an event	Incremental mean intensity EC and $\delta^{18}O$ values per event (as bulk samples)	Average EC and $\delta^{18}O$ of samples taken during the winter baseflow period (December to March)
B	Time-invariant	Average EC and $\delta^{18}O$ of supraglacial meltwater samples taken during the ablation season (July to September)		
C	Time-variant at subdaily scale (only for events #5 and #6)	EC and $\delta^{18}O$ of individual supraglacial meltwater samples taken during an event (before noon, around noon, and afternoon)		
D	Spatially variable (local scale; spatial extent <1,400 m)	EC and $\delta^{18}O$ of individual supraglacial meltwater samples taken at various locations		

Note. EC = electrical conductivity.

TABLE 2 Hydro-climatologic conditions during the study period

	Discharge (m^3/s)				Air temperature (°C)				Precipitation (mm)			Spearman correlation coefficient (*p* value)
Date	Min	Mean	Max	CV	Min	Mean	Max	CV	During the event	2 days prior to the event	7 days prior to the event	
2016-07-19	1.06	2.26	4.35	0.47	4.93	8.92	12.55	0.31	0	0.2	58.9	.46 (.02)
2016-07-30	1.36	2.77	4.26	0.37	5.65	8.77	12.37	0.26	1	0.2	19.2	.58 (<.01)
2016-08-08	0.49	1.25	2.58	0.56	5.65	8.07	11.02	0.23	0	0.4	49.2	.39 (.06)
2016-08-31	1.04	2.79	5.40	0.54	4.40	6.90	9.82	0.27	4	15.3	48.7	.59 (<.01)
2016-09-13	0.77	2.17	4.41	0.66	4.45	7.00	9.77	0.24	0	5.9	25.9	.51 (.01)
2016-09-22	0.34	0.40	0.54	0.17	−1.75	1.91	5.62	0.71	0	2.8	18.9	.23 (.29)
2015-12-01 to 2016-03-31	0.04	0.06	0.10	0.24	−23.90	−7.10	4.45	0.67	268	—	—	.40 (<.01)

Note. Temperature and precipitation were measured at the "Latschbloder" weather station and discharge was measured at the gauging station "Bridge." The Spearman correlation coefficient describes the relation between discharge and air temperature.

during the ablation period (July to September) were characterized by distinct diurnal cycles in air temperature and discharge (Figure 2b–g). The highest variation in discharge was observed for event #5 (CV = 0.66). Mean values for event air temperature ranged between 1.9 °C (for event #6) to 8.9 °C (for event #1). Average event discharge was between 0.40 (event 6#) and 2.79 m^3/s (event #4). A significant correlation was observed between discharge and air temperature for the events #1 to #5, with Spearman correlation coefficients ranging between .39 (event #3) and .59 (event #4) at 10% significance level (Table 2). Events #1, #3, #5, and #6 were rain-free, and all events were at least dominated by clear sky and high radiative energy input. Rainfall was observed during event #4 (3.9 mm) and event #2 (0.9 mm). API_2 was highest for event #4 (15.3 mm) and smallest for events #1 and #2 (0.2 mm). Maximum API_7 was observed for event #1 (58.9 mm), and a minimum value was observed for event #6 (18.9 mm, Table 2).

4.2 | Tracer variability in water sources and streamflow

All analysed water samples are split into water sources (glacier melt, groundwater, rain) and streamflow in Figure 3. Rain $\delta^{18}O$ values are higher compared with glacier melt, groundwater, and streamflow $\delta^{18}O$ values (Figure 3a). Rain isotopic values are significantly different from glacier melt (Kruskal–Wallis test: $p < .001$) and groundwater (Kruskal–Wallis test: $p = .002$). Figure 3b displays low EC values for rain and glacier melt, high ones for groundwater and intermediate ones for streamflow. There are significant differences in EC between each of the three water sources observed (pairwise Wilcoxon test with post hoc Bonferroni correction: $p < .001$). The groundwater (winter baseflow) tracer signatures ($n = 14$) were spread between −14.7‰ and −14.5‰ (median = −14.6‰) for $\delta^{18}O$ and between 175.2 and 186.0 µS/cm (median = 184.1 µS/cm) for EC. The variation throughout the December to March period and for an intense sampling day on March 17 ($n = 9$, 30-min interval) was small for both analysed tracers (Figure 3, Table 3). The variation of rain samples ($n = 9$) collected during the July to September period was observed for EC and $\delta^{18}O$ (Figure 3, Table 3). Values for EC range from 4.7 to 14.5 µS/cm (median = 7.4 µS/cm). $\delta^{18}O$ data range between −17.7‰ to −5.3‰ (median = −8.8‰). Streamflow samples ($n = 19$) collected during the events were varying between −14.1‰ and − 13.4‰ (median = −13.8‰) for $\delta^{18}O$ and between 45.8 and 158.3 µS/cm (median = 89.4 µS/cm) for EC. Discharge reveals a strong relationship to tracer signatures of streamflow (Figure 4a,b). The discharge is positively correlated with $\delta^{18}O$ (Kendall's Tau: $\tau = 0.69$, $p < .001$) and negatively with EC (Kendall's Tau: $\tau = -0.58$, $p < .001$). Data for event #6 (green circles) stand out for both relationships and are characterized by relatively low discharge and relatively high EC and low $\delta^{18}O$ values. These data therefore form a distinct cluster.

Glacier melt samples ($n = 51$, Table 3, Figure 5) ranged from −17.0‰ to −12.2‰ in $\delta^{18}O$ (median = −14.7‰) and from 1.3 to 10.1 µS/cm in EC (median = 2.1 µS/cm). The inter-event variability was marked for both EC and $\delta^{18}O$, and medians of event #6 values

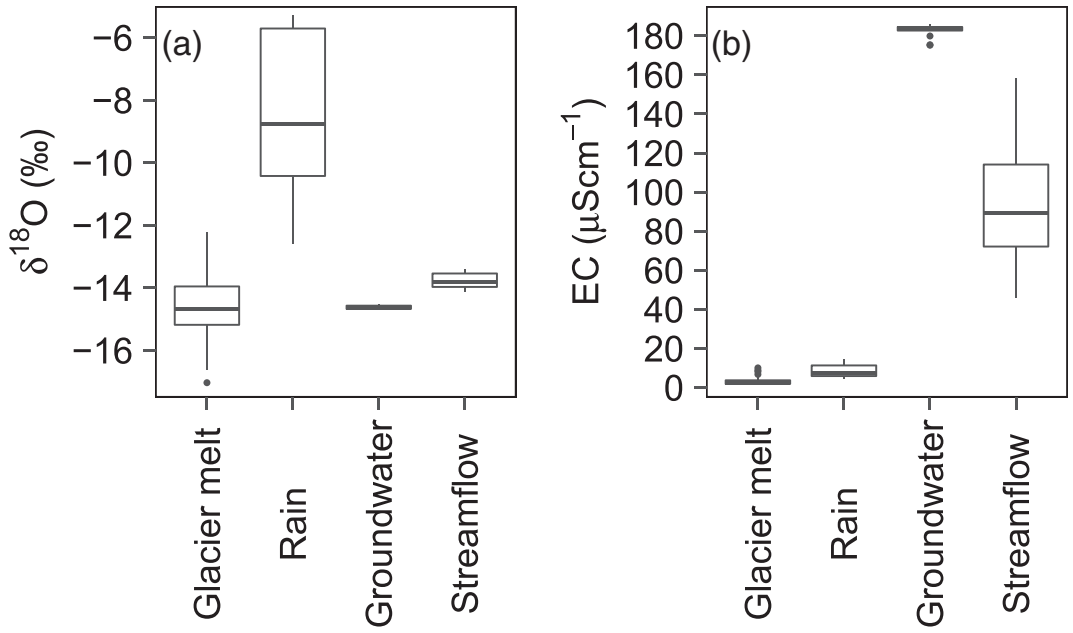

FIGURE 3 $\delta^{18}O$ (a) and EC (b) signatures of water sources and streamflow. EC = electrical conductivity

TABLE 3 Descriptive statistics of tracer signatures for water sources and streamflow

		EC (µS/cm)					$\delta^{18}O$ (‰)				
	N	Min	25th percentile	Median	75th percentile	Max	Min	25th percentile	Median	75th percentile	Max
Groundwater	14	175.2	182.7	184.1	184.5	186.0	−14.7	−14.7	−14.6	−14.6	−14.5
Rain	9	4.7	5.9	7.4	11.4	14.5	−17.7	−11.8	−8.8	−5.8	−5.3
Glacier melt	51	1.3	1.9	2.1	3.7	10.1	−17.0	−15.2	−14.7	−14.0	−12.2
Streamflow	19	45.8	72.2	89.4	114.1	158.3	−14.1	−14.0	−13.8	−13.5	−13.4

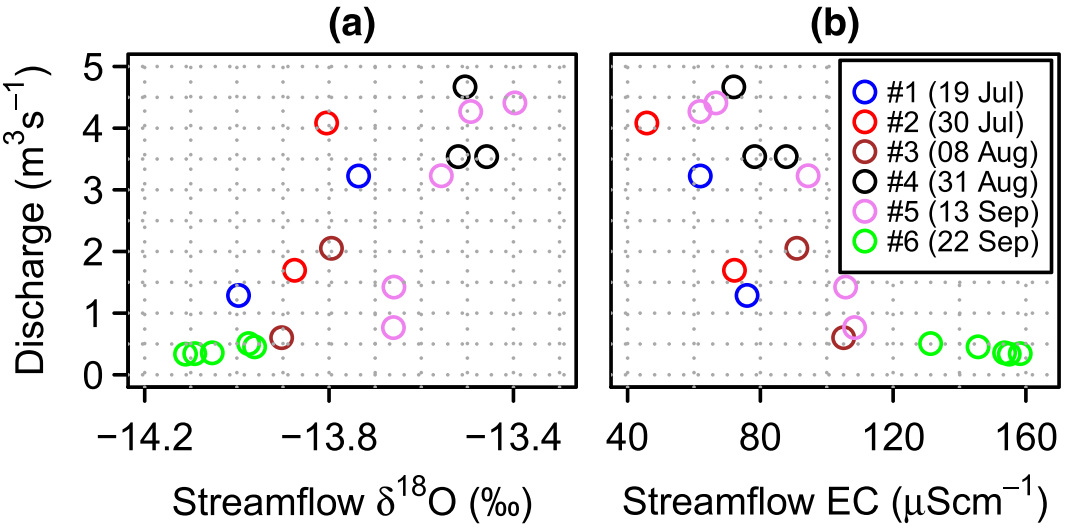

FIGURE 4 Relationship of discharge to streamflow $\delta^{18}O$ (a) and EC (b) during the investigated events. EC = electrical conductivity

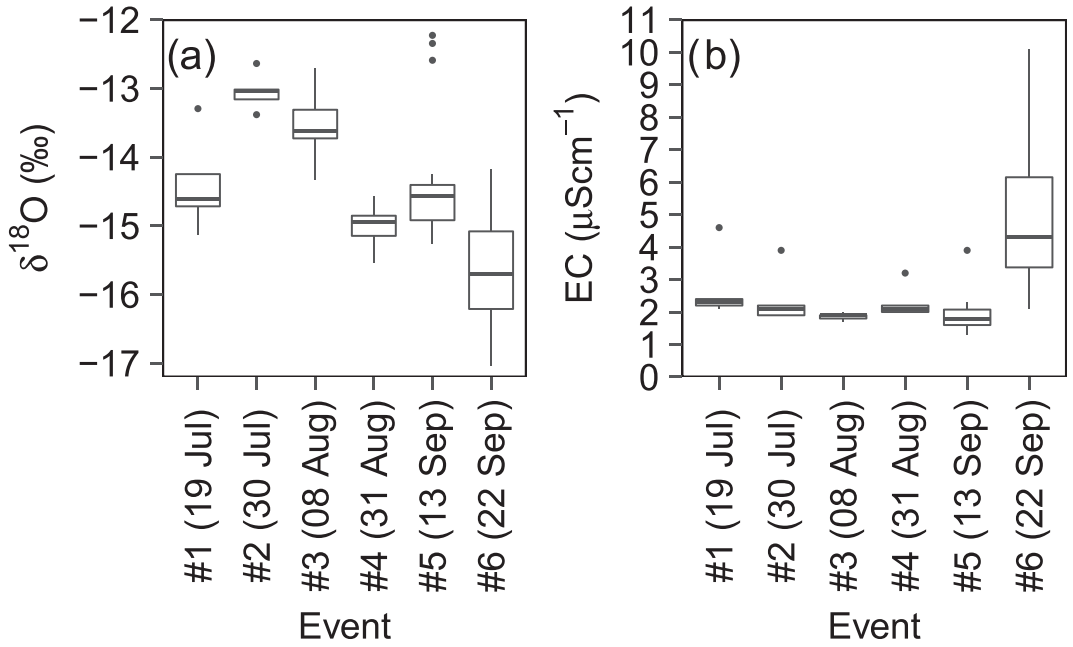

FIGURE 5 $\delta^{18}O$ (a) and EC (b) signatures of glacier melt during the investigated events. EC = electrical conductivity

were statistically different to most of the remaining event values at 10% significance level (pairwise Wilcoxon test with post hoc Bonferroni correction). The temporal intra-event variability (data from events #5 and #6) was significantly different for EC on September 13 (10:00 and 13:00 values differed with p = .003) but not for $\delta^{18}O$. Kruskal–Wallis tests on medians of different sampling sites for events #1 to #4 (sampling sites A1 to A5) and for events #5 and #6 (sampling sites A1 to B3) revealed no statistical significant difference for EC and $\delta^{18}O$. Tests in tracer signature differences for both investigated glacier tongues (A, B, cf. Figure 1) revealed no statistical significant differences (Kruskal–Wallis for EC and $\delta^{18}O$). The temporal variation and the spatial variation between the sampling locations in tracer signatures of glacier melt are displayed in Figure 6. There is no clear spatial pattern observable, and the colour variation along the x-axis (i.e., temporal variability) seems to be larger compared with the one along the y-axis (i.e., spatial variability). EC values (Figure 6b,d) display at the lower end of the colour range (more blueish pixels) whereas $\delta^{18}O$ values seem to cover the colour range (from blue to red) more evenly distributed over the whole observation period (Figure 6a,c). The glacier melt $\delta^{18}O$ values at A1 on September 13 (reddish pixels in Figure 6c), as well as the higher varying EC values on September 22 (blue to red pixels in Figure 6d) compared with the remaining EC values stand out.

4.3 | Hydrograph separation results and their uncertainties

The end-members glacier melt, groundwater, and rain span a triangle around the stream samples in the EC-$\delta^{18}O$ mixing space and allow for applying a three-component mixing model (Figure 7; end-member

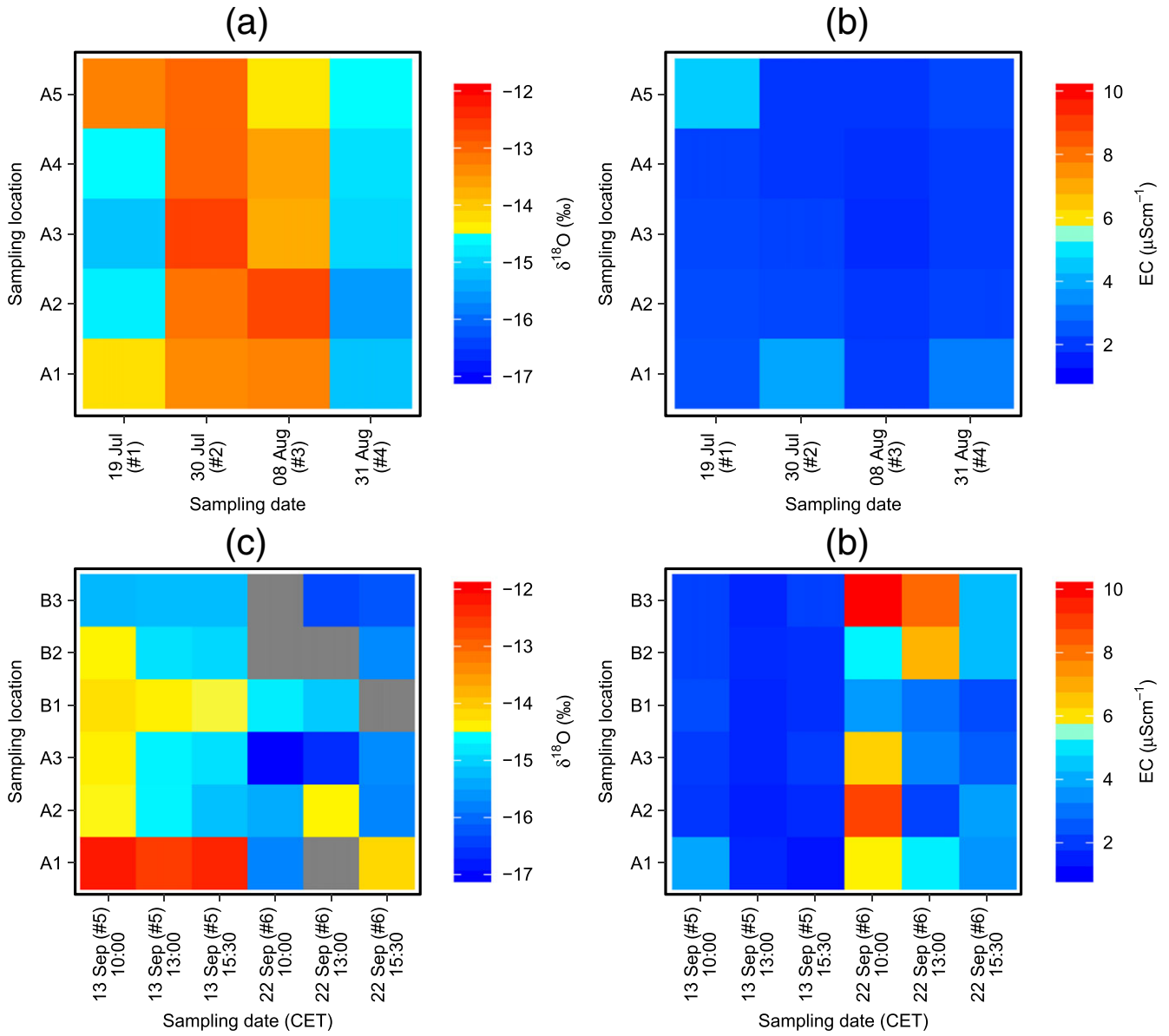

FIGURE 6 Spatio-temporal pattern of glacier melt sampled on events #1 to #4 for $\delta^{18}O$ (a) and EC (b), and $\delta^{18}O$ (c) and EC (d) glacier melt signatures for events #5 and #6. Grey pixels indicate missing data. EC = electrical conductivity

values for the different events are shown in Table S3). The event #6 streamflow samples (green circles) group apart from the main cluster (event #1 to #5) and are located closer to the groundwater end-member in the mixing space. Figure 8 displays the average streamflow component fractions and associated uncertainties per event, estimated with the mixing model and Approach A (mean glacier melt end-member tracer signature per event). It becomes obvious that streamflow is composed differently in each event, and this reflects the variability throughout the ablation period. The lowest mean glacier melt fraction was observed for event #6 (5±5%) and was accompanied by the lowest air temperatures (mean daily air temperature: 1.9 °C). The highest mean glacier melt fraction was observed for event #2 (69±10%), concomitant with the highest runoff (14 mm). The median glacier melt fraction of all six events was 35±11%. The average rain fraction of streamflow per event ranged between 0±10% (event #2) and 23±6% (event #4) with a median of 16±11% for all events. The mixing model applied for event #2 revealed no rain contribution to streamflow. Hence, we conducted a two-component hydrograph separation with EC (Pinder & Jones, 1969) for event #2 that revealed a mean glacier melt fraction of 69±2%. The maximum rain contribution (24±6%) was observed during event #4 (12:00 CET). The median groundwater contribution to streamflow for all events was 49±2%. Mean fractions per event ranged between 31±2% (event #2) and 81±3% (event #6). A maximum fraction (86±4%) was estimated for event #6 (11:00 CET) and a minimum fraction (24±1%) for event #2 (14:00 CET). The glacier melt fraction was also varying at the subdaily scale (Figure 9). The glacier melt fraction shows a similar pattern for each event, that is, an increase over the course of the day with a maximum range observed for event #5 (increase from 24±11% to 48±20%). Subdaily glacier melt fractions ranged between 2±5% (September 22, 11:00 CET) and 76±11% (July 30, 14:00 CET), and the highest uncertainty was estimated for event #5 (up to ±20%).

Figure 10 shows the sensitivity of the estimated glacier melt fractions to the sampling time of glacier melt (Approach C). The

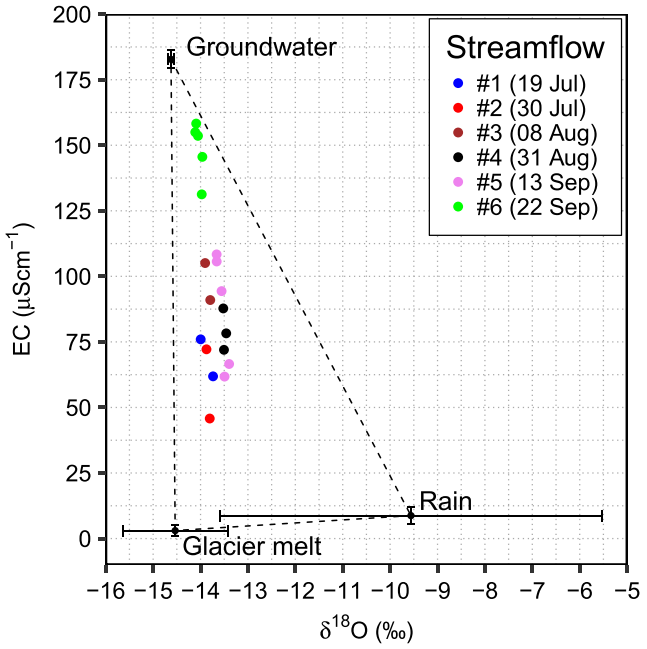

FIGURE 7 EC–$\delta^{18}O$ mixing plot. The end-members (rain, glacier melt, groundwater) are represented by mean values (error bars indicate the standard deviation) and span a triangle around the streamflow samples. EC = electrical conductivity

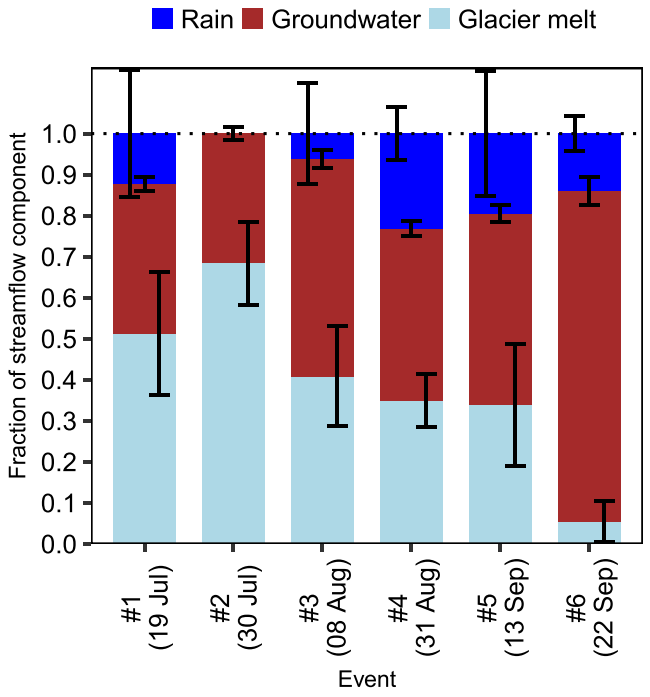

FIGURE 8 Average streamflow component fraction and uncertainty (error bars) per event (estimated with Approach A)

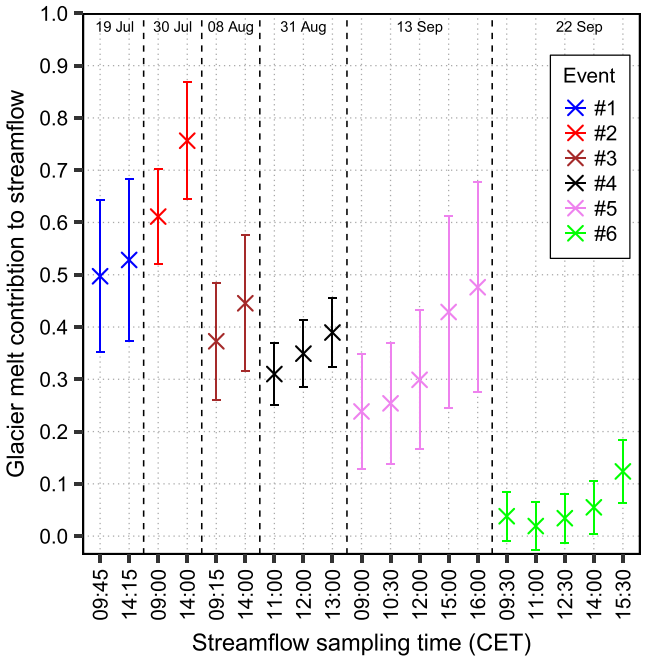

FIGURE 9 Glacier melt fraction and uncertainty (error bars) estimated with Approach A. Please note that *x*-axis scale is not continuous

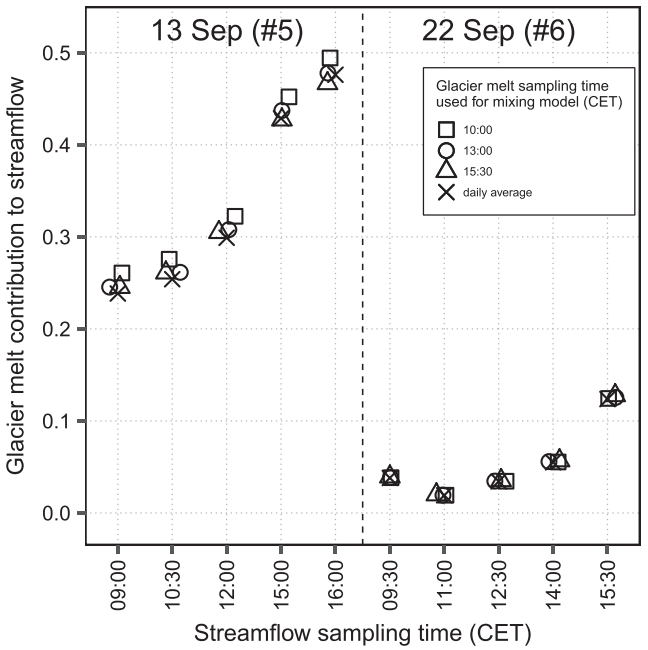

FIGURE 10 Sensitivity of estimated glacier melt contribution to subdaily glacier melt end-member characterization (Approach C) for events #5 and #6. Crosses represent glacier melt fractions estimated with Approach A. Please note that *x*-axis scale is not continuous

variations are not marked, and the values are close to the Approach A values (represented by crosses in Figure 10), but event #5 (September 13) reveals a slightly higher spread compared with event #6 (September 22). During event #5, the glacier melt sampling time before noon (10:00 CET) led to slightly higher glacier melt contributions compared with the average value (Approach A; for the exact values, see Table S1). Figure 11 highlights the sensitivity of the estimated glacier melt fractions to the sampling location of glacier melt (Approach D). Overall, the scatter around the average value (results from Approach A) is limited (<7% absolute difference), except for event #1 (sampling location A5) and event #5 (sampling location A1) an outlier appears. A maximum absolute difference of +15% and +24% for both events was calculated, respectively (exact values are shown in Table S2). Figure 12 shows the glacier melt contribution to streamflow and

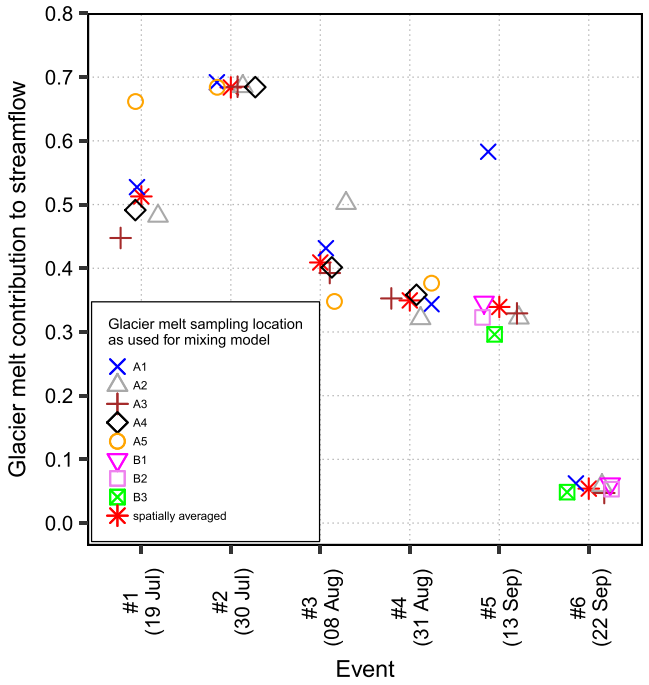

FIGURE 11 Sensitivity of estimated glacier melt contribution to the glacier melt sampling location (Approach D). Red stars represent glacier melt fractions of Approach A. Please note that *x*-axis scale is not continuous

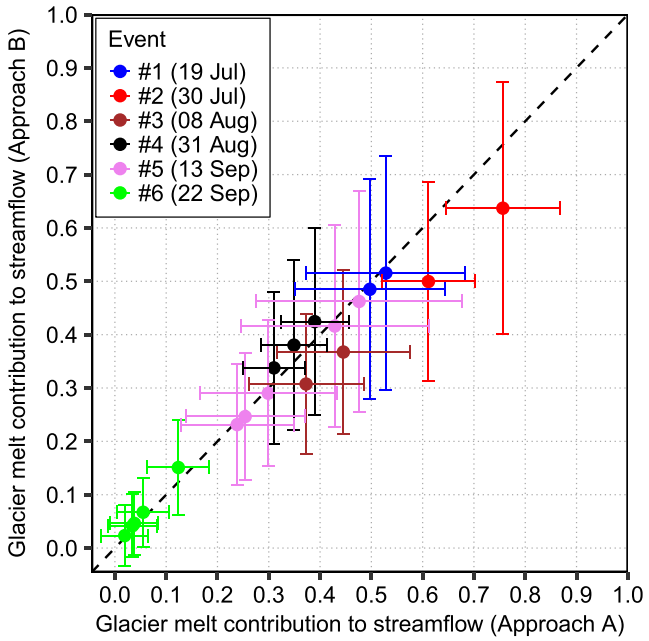

FIGURE 12 Comparison of glacier melt fraction and uncertainty estimated with Approach A and B

associated uncertainties estimated with Approach B (mean seasonal glacier melt end-member tracer signature) against those estimated with Approach A (mean event glacier melt end-member tracer signature). Glacier melt fractions estimated with Approach B revealed on average 5% lower glacier melt fractions compared with those of Approach A. Glacier melt fractions estimated with Approach B revealed similar estimates (close to the 1:1 line in Figure 12) for events #1, #4, #5, and #6. Maximum deviations were observed for events #2 and #3 (−17% of Approach A value).

The mean rain fraction of streamflow during the events is positively correlated with API_2 (Kendall's Tau: $\tau = 0.73$, $p = .06$) but not with API_7. The rain fraction of streamflow has a positive relationship with $\delta^{18}O$ (Kendall's Tau: $\tau = 0.54$, $p < .001$) but none with EC. The groundwater fraction of streamflow is correlated with EC (Kendall's Tau: $\tau = 0.99$, $p < .001$) and $\delta^{18}O$ (Kendall's Tau: $\tau = -0.52$, $p < .001$). The mean fraction of glacier melt during the event is positively correlated with mean event air temperature (Kendall's Tau: $\tau = 0.73$, $p = .06$). The relationship between glacier melt fraction (Approach A) and streamflow tracer signatures is displayed in Figure 13a,b. The glacier melt fraction is positively correlated with streamflow $\delta^{18}O$ (Kendall's Tau: $\tau = 0.32$, $p = .06$) and negatively correlated with EC (Kendall's Tau: $\tau = -0.81$, $p < .001$). The data in the scatterplot show the event-wise grouping for both tracers (see colour-coding of the events).

5 | DISCUSSION

5.1 | Tracer variability in water sources and streamflow

The spatio-temporal variability in tracer signatures of water sources represents a large source of uncertainty in applying mixing models (Pu et al., 2013; Uhlenbrook & Hoeg, 2003). Therefore, adequate sampling strategies (e.g., not sampling peak flow or sampling during wet antecedent days potentially leads to underestimated glacier melt fractions) are necessary for the planning of field campaigns, as already noted by Penna et al. (2017). Sampled water sources (glacier melt, rain, and winter baseflow as a proxy for shallow groundwater) revealed significant differences in EC and marked differences in $\delta^{18}O$ (Figure 3). EC is a proxy for total dissolved solids and was relatively high in shallow groundwater. This suggests that the catchment hydrology is dominated by slower, subsurface flow paths of water during the December to March period. Little variation in $\delta^{18}O$ values of stream discharge (−14.7‰ to −14.5‰) during this period also supports the evidence of a well-mixed groundwater reservoir that supplies winter baseflow similar to Ambach et al. (1976), Penna et al. (2017), and Rodriguez et al. (2016). Lower EC values were observed in the Hochjochbach stream during the summer ablation period (July to September) compared with the EC values during the winter baseflow period (Figure 3b). Higher EC values during winter and lower values in summer are typical for glacierized catchments (e.g., Penna et al., 2017). This indicates marked contributions of glacial meltwater, which is typically diluted in solutes (Figure 3b). During the events (July to September), streamflow $\delta^{18}O$ varies between −14.1‰ and −13.4‰ and indicates changing contributions of water sources with different signatures. Analogously, the varying EC content of streamflow (range: 45.8–158.3 µS/cm) indicates the contribution of high EC groundwater or the low EC rain/glacier melt component, under the assumption of homogenous geology and flow paths. The negative relation between discharge and streamflow EC (dilution effect) in melt-dominated catchments was already intensively studied (Collins & Young, 1981;

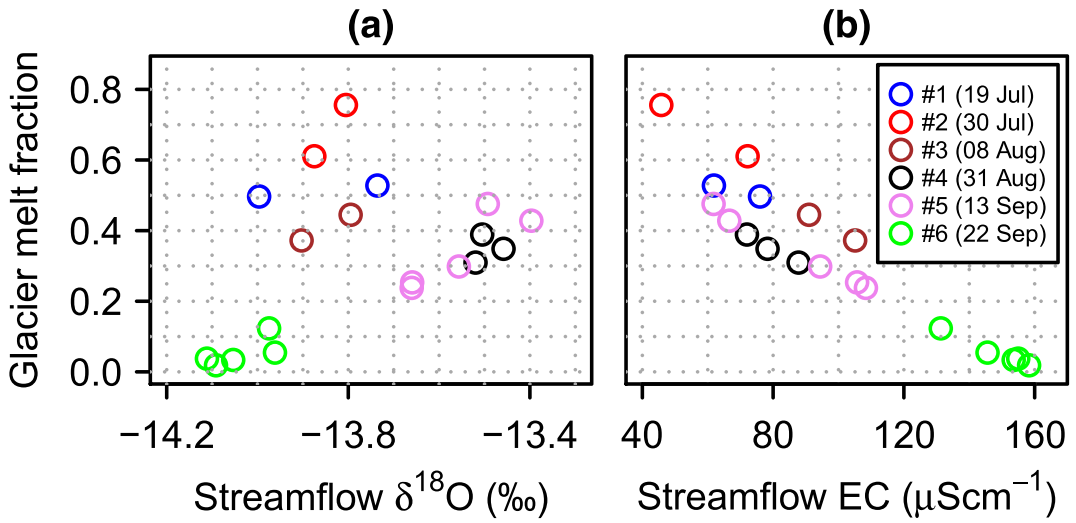

FIGURE 13 Relationship between glacier melt fraction (Approach A) and streamflow $\delta^{18}O$ (a) and EC (b). EC = electrical conductivity

Dzikowski & Jobard, 2012; Engel et al., 2016) and was also significant within this study (Figure 4b). A significant positive relationship of discharge and streamflow $\delta^{18}O$ was found (Figure 4a). Spatio-temporal variation in rain isotope signatures (Figure 3a) is observed (range between −17.7‰ and −5.3‰) but is not the main interest in this study. EC of rain varies between 4.7 and 14.5 µS/cm, most likely varying due to air masses originating from Mediterranean (favours more salty rain and higher EC values) or Atlantic (favour less salty rain and lower EC values) moisture sources. Variations in EC of rain may also occur due to atmospheric deposition (e.g., dust). Penna et al. (2014) also observed a similar range in EC of rain in a catchment close to our study area.

The sample size (n = 51 in total) of this study to characterize the glacier melt tracer signature is one order of magnitude greater compared with most other studies and therefore allows to draw a solid conclusion on the temporal and spatial variability (at the local scale). The temporal variability in glacier melt tracer signature was higher compared with the spatial variability. The intraseasonal variation was larger compared with the within-day variation for $\delta^{18}O$. A decreasing tendency in the isotopic composition of glacier melt from events #2 to #6 is visible, which is contrary to the findings of Penna et al. (2017) and Yde et al. (2016), who observed an increase in glacier melt isotopic signatures during the ablation period. Other authors found no intraseasonal variability in glacier melt tracer signatures (Cable et al., 2011; Maurya et al., 2011; Ohlanders, Rodriguez, & McPhee, 2013; Racoviteanu, Armstrong, & Williams, 2013). The within-day variability in EC and $\delta^{18}O$ was marked for event #6; however, this variability was not observable during the other events (Figure 5). The high variation is likely related to an intermittent snowfall event, where a thin layer (<2 cm) of new snow covered the Hochjochferner (all snow was melted in the afternoon). Typically, snow is characterized by lower $\delta^{18}O$ values due to the temperature effect (Dansgaard, 1964). The intradaily variation in EC of glacier melt on September 22 was likely caused by the dilution effect. Due to the low radiative energy input, the resulting melt rate was low in magnitude, which was visually ensured. At 10:00 (CET) when melt was minimal, meltwater draining from the abovementioned new snow on the glacier surface, which is typically higher in EC compared with glacier meltwater (Fountain, 1996), led to relatively high EC values (yellow to reddish pixels in Figure 6d). These became progressively lower with a minimum at 15:30 (CET) in the afternoon when the melt rate was highest. Jeelani et al. (2017) found higher EC values in meltwater originating from a debris-covered glacier compared with a clean glacier. Because glacier melt tracer signatures depend on the water origin (e.g., supraglacial meltwater vs. glacier outflow), the origin of the air masses that form precipitation and the post-depositional processes, a direct comparison is solely valuable for catchments with similar climate conditions and physical characteristics. As an example, Penna et al. (2014) sampled rivulets on the glacier surface in a catchment close to the Hochjochbach catchment and revealed medians of approximately −14‰ and 5 µS/cm for $\delta^{18}O$ and EC (extracted from figure), respectively, which are close to our values. A small spatial variation but a marked intraseasonal pattern in the tracer signature of glacier melt was observed by Penna et al. (2017). A clear intraseasonal enrichment of glacier melt isotope values could not be identified within this study, but a variation that should be accounted for in mixing models was observed (Figure 5). The spatial variation was negligible (Figure 6) but should be investigated at a larger spatial scale, although assumptions exist on missing isotope variability of different glaciers within a catchment (Cable et al., 2011). S. Zhou, Wang, and Joswiak (2014) found no clear altitude gradient in the isotopic signal of glacier melt, whereas Wu et al. (2016) found an altitude effect (−0.34‰/100 m for $\delta^{18}O$). For the Hochjochferner, this would result in a total change of −2.38‰/700 m. This effect, if observed, would play a minor role because the value lies within the observed range of the Hochjochferner glacier melt values and most of the glacier melt originates from the ablation area (glacier tongue), where the sampling was conducted. Despite our efforts to capture the variability in the glacier melt tracer signature, identification of it at a larger spatial scale (sampling various glaciers in a catchment >20 km^2) remains an open issue. Future work is also required in estimating the interannual variability of the glacier melt tracer signature.

5.2 | Hydrograph separation results and their uncertainties

In a variety of mountain catchments worldwide and different mixing model settings, subsurface water, rain, and melt contributions to streamflow at the seasonal scale were quantified by 2–76, 20–22, and 13–53%, respectively (e.g., Cable et al., 2011; Zhou et al., 2015). Nevertheless, those studies are often hard to compare due to (a) different glacier melt definitions (Frenierre & Mark, 2014), (b) differences in glacierized area, (c) climate variability, (d) spatio-temporal scale issues (Penna et al., 2017), (e) varying characterization of end-members (e.g., predetermined or determined by geochemical streamflow data), and (f) sampling of different components (e.g., sampling glacial outflow vs. supraglacial meltwater to characterize the glacier melt end-member or sampling winter baseflow vs. spring water to characterize the groundwater end-member).

5.2.1 | Glacier melt fraction in streamflow and its sensitivity to the glacier melt end-member characterization

The median glacier melt contribution to streamflow for six events during July to September was 35±11% and was in the range of seasonal glacier melt contributions (28–59%) estimated in other studies for similar catchments (Cable et al., 2011; Engel et al., 2016; Penna et al., 2017). If one assumes that annual glacier melt contribution occurs solely within the July to September period and runoff constitutes of 35% glacier melt (367 mm) during that period, glacier melt contributes approximately 23% to annual runoff (1619 mm) in the Hochjochbach catchment (October 2015 to September 2016). Maximum event contribution was 69±10% (event #2) and compares well with maximum estimates from Penna et al. (2017) and Engel et al. (2016) at the event scale (71% and 65%, respectively). This represents the importance and dominance of the glacier melt streamflow fraction in headwater catchments during summer in the Alps, and future changes in glacial meltwater contribution in that region are likely (e.g., Hanzer, Förster, Nemec, & Strasser, 2017). A dominant role of glacier melt in summer and late summer streamflow was also observed in the Rocky Mountains (Cable et al., 2011), Andes (Ohlanders et al., 2013), and the Arctic (Blaen, Hannah, Brown, & Milner, 2014). In this study, a decreasing pattern in glacier melt fraction was observed from July 30 (69±10%, event #2) to September 22 (5±5%, event #6). This dynamic behaviour was contrary to the findings of Williams et al. (2016) and Racoviteanu et al. (2013) who revealed an increase in glacier melt contribution for the July to September period in the Himalaya. Our observed pattern could be related to the observation period, starting when snow cover was almost depleted and annual peak glacier melt likely occurred close to the beginning of the summer sampling work (end of July) and was followed by a subsequent recession of the glacier melt contribution. Penna et al. (2017) also observed most of the glacier mass loss between end of July and mid-August. Further estimates on the interannual glacier melt contribution variability are required. The relatively high uncertainty during event #5 (up to ±20%; see Figure 9) is likely caused due to a combination of the highly varying glacier melt $\delta^{18}O$ signature and a high glacier melt fraction (up to 48%), both affecting the uncertainty estimation (cf. Genereux, 1998). The mixing model results were partly sensitive to the characterization of the glacier melt end-member. Using the seasonal average of the glacier melt tracer signature for applying the mixing model (Approach B) led to underestimated glacier melt fractions (average: −5%) compared with the use of the event mean glacier melt tracer signature (Approach A), especially when glacier melt was the dominant contributor. Hence, the highest deviation was observed for events #2 and #3 (−17%). We infer that it is necessary to use a time-varying glacier melt end-member at least at the subseasonal scale as already done recently by Penna et al. (2017) and Wu et al. (2016) at the monthly scale. Furthermore, our data show that it is important to incorporate the temporal variability of glacier melt tracer signature below a monthly resolution, because the $\delta^{18}O$ values to describe the glacier melt end-member (Figure 5) varied from event to event. However, the sensitivity of the glacier melt contribution to the subdaily characterization of the glacier melt end-member (Approach C) is not marked. There is a small deviation observable if one samples glacier melt in the morning (10:00 CET) (event #5 in Figure 10). This effect is caused by the higher $\delta^{18}O$ values (yellow pixels in Figure 6c) compared with those at 13:00/15:30 (CET). This was not the case for event #6, and we want to point out that those two events are likely not sufficient to draw a general conclusion of such an emergence as observed for event #5. Hence, we hypothesize that the subdaily variation of the glacier melt end-member tracer signature may not be important, but further data from different catchments are absolutely needed to test it. The sensitivity of the glacier melt estimations to the spatial variability of the glacier melt tracer signature (Figure 11) is also not marked, but two outliers (sampling locations A1 and A5) become obvious. Both, for event #1 the sampling location A5 and for event #5 the sampling location A1, led to markedly higher glacier melt estimates compared with the average value. Both cases were caused by high $\delta^{18}O$ values (cf. Figure 6). We cannot explain the abovementioned outliers, but our data showed that sampling either at different locations on the ablation area, or sampling both tongues of the glacier (cf. Figure 1 and Section 2) does not seem to be of particular importance. The correlation of the glacier melt fraction of Approach A and the streamflow tracer signature were significant for both $\delta^{18}O$ and EC at 10% significance level (Figure 13). The observed relationship is stronger for the glacier melt fraction and streamflow EC, similar to the dilution effect described in other studies (e.g., Dzikowski & Jobard, 2012). The less strong relationship between streamflow $\delta^{18}O$ and the glacier melt fraction (Figure 13a) could likely be attributed to the similarity of the glacier melt and the groundwater $\delta^{18}O$ values (cf. Figure 3 and Table 3). However, data for events #1 to #3 seem to deviate from the relationship for both, EC and $\delta^{18}O$.

5.2.2 | Groundwater fraction in streamflow and its end-member characterization

Groundwater, characterized by the winter baseflow tracer signature was the dominant contributor to streamflow (49±2%) for the studied six melt events during the period July to September 2016. At the event scale, we observed an increase in groundwater contribution to streamflow from event #2 (31±2%) to event #6 (81±3%) that is inversely related to the glacier melt contribution. Engel et al. (2016)

determined groundwater contribution up to 62% for melt events analysed in a small headwater catchment (12% glacierized area) in the Alps and found that groundwater was the major streamflow component for seven observed melt events (38% to 62%). Penna et al. (2017) investigated a tendency of increasing groundwater contribution between July and September in the same catchment, with a maximum contribution >80% (approximate value extracted from figure). Large groundwater contributions and its storage in soils and unconsolidated sediment (such as talus, moraines, alluvium, alluvial fans, and rockslides) are frequently observed in high-elevation catchments and likely play a major role for future water supply, especially under changing climatic conditions and system states of those catchments (Jasechko, Kirchner, Welker, & McDonnell, 2016; Staudinger et al., 2017). Baseflow is a combination of shallow and deep groundwater (Ward & Robinson, 2000), can have long residence times (Ambach et al., 1976; Stewart & McDonnell, 1991), and is a mixture of snowmelt, rain, and glacier melt, as quantified by Cable et al. (2011). There was an intense discussion on the characterization of the subsurface end-member as condensed by Buttle (2006). Characterizing the groundwater end-member by the tracer signature of (winter) baseflow can be more reliable than using averaged spring water, because the isotopic and geochemical signature of streamflow during baseflow conditions is known to integrate and represent the hydrochemistry of (shallow) groundwater at the catchment scale (Fischer, Rinderer, Schneider, Ewen, & Seibert, 2015; Kendall & Doctor, 2003; Klaus & McDonnell, 2013; Sklash, 1990). Nevertheless, using winter baseflow instead of average spring water tracer signatures could lead to underestimated glacier melt fractions, as shown by Penna et al. (2017). We considered winter baseflow tracer signature to characterize the groundwater end-member, as used elsewhere (e.g., Miller, Buto, Susong, & Rumsey, 2016). Because small mountainous headwater catchments typically tend to favour shallow subsurface flow paths (Frisbee, Phillips, Campbell, Liu, & Sanchez, 2011), whereas deeper longer flow path bypass first-order (headwater) streams through fractured bedrock and supply stream water at a larger scale downstream (Gleeson & Manning, 2008), the groundwater end-member is considered to represent shallow subsurface flow in this study. Unconsolidated material such as glacial deposit, moraine, till, and loose rock of talus slopes likely functions as storage of this water source, which is not negligible in high-elevation catchments as the Hochjochbach basin. Accounting for the temporal variation of the groundwater tracer signature is difficult, but a distinct variation could not be shown within this study. Therefore, the use of the (time-invariant) average tracer signature of winter baseflow during the December to March period seemed reliable to characterize the groundwater end-member.

5.2.3 | Rain fraction in streamflow and inferred runoff mechanisms

The median rain fraction in streamflow during the six investigated events was estimated at 16±11%. Minimum and maximum event contribution was 0±10% (event #2) and 23±6% (event #4). Dahlke et al. (2014) investigated rainfall–runoff events in a 30% glacierized catchment (21.7 km^2) in Northern Sweden with very similar characteristics and climate as the Hochjochbach catchment using a two-component hydrograph separation with $\delta^{18}O$. The event water end-member was characterized by rain samples and was on average 11% and 22% for two nonconsecutive ablation periods, depending on interplay between the rainfall event timing, snow cover, and soil moisture conditions. Related rain contributions during melt-induced events are very rare hence a comparison is hampered. As an example, Engel et al. (2016) estimated a marked rain contribution of 11% for a rainfall–runoff event (<10 mm/day precipitation) by a two-tracer (EC and $\delta^{18}O$) three-component mixing model (rain, glacier melt, groundwater), well comparable with our results and highlighting the importance of rain contribution in glacierized catchments. It should be mentioned that our results were related to antecedent rainfall. Because rainfall–runoff dynamic was not the major part of interest in this study and sampling was conducted on almost rain-free events (except on events #2 and #4 rainfall occurred, but sampling on those days was finished before), our estimated rain fractions in the streamflow are not negligible. The correlation analysis of the 2-day antecedent rainfall sum and the rain fraction of streamflow were significant and support the assumption of longer transit times (longer than 1 day as assumed for the glacier melt end-member). Two-day residence time is short but seems reasonable due to thin soils and unconsolidated material (deposit, moraine), which likely favours a higher hydraulic conductivity (see Weiler, McDonnell, Van Meerveld, & Uchida, 2005). Baraer et al. (2015) underscored in their Andean catchment the importance of groundwater contribution in proglacial regions and suggested talus deposits as controlling landscape features that regulate shallow groundwater movement and routing of rain water through the subsurface. This is also typical for the Hochjochbach catchment. Therefore, including the rain component is crucial in glacierized catchments. Furthermore, the EC-$\delta^{18}O$ mixing diagram (Figure 7) indicates that streamflow tracer signature cannot be explained by using one tracer only (streamflow samples display not on a line between two water sources). Glaciers are known to have a low retention capacity for rain water (especially if the snow cover is depleted) and provide a fast routing of rainwater to the stream (Dahlke et al., 2014). Due to this fact and the investigation of antecedent (not event) rainfall–runoff dynamics, we must conclude that catchment storage (not glacier storage) is the key to better understand rainfall–runoff dynamics in glacierized catchments at a scale that is larger than one day. Future work on the relation between rainfall and runoff should be conducted in those environments.

6 | CONCLUSION

In this study, we presented novel research including (a) winter baseflow tracer variation in a glacierized catchment, (b) high temporal and spatial resolution of the glacier melt tracer signature (large dataset), and (c) tracer-based streamflow partitioning (glacier melt, rain, groundwater) and its sensitivity to the glacier melt tracer variability. Our work is representative for headwater catchments (30–40% glacier coverage) with a glacial flow regime. We investigated six melt-induced events during the ablation period from July to September 2016 in a 17.1 km^2 catchment (34% glacierized area) in the European Alps and assessed the spatio-temporal variability of end-member tracer signatures ($\delta^{18}O$, EC). The winter baseflow tracer signatures

served as a proxy for shallow groundwater and revealed a very small variation, supporting the evidence of a well-mixed reservoir. The temporal tracer variation of glacier melt (EC and $\delta^{18}O$) is marked at the subseasonal scale (July to September) and is more pronounced for $\delta^{18}O$. Subdaily and spatial variation plays a minor role, but also variations in $\delta^{18}O$ are more pronounced. The glacier melt fraction at the daily (event) scale ranged between 5±5% and 69±10% (median: 35±11%), with an annual contribution of 23%, that likely represents the lower threshold. Groundwater (median: 49±2%) was the dominant contributor during the investigated events, likely becoming more important due to further retreat of the glacier and expected future decrease in the glacier melt contribution. Antecedent rain played a minor but not negligible role (median: 16±11%). We have shown that including a time-variant glacier melt end-member characterization (if possible at the submonthly scale) in mixing models is important, because using a time-invariant glacier melt tracer signature led to 5% lower glacier melt fractions on average and up to 17% underestimation per event. Spatial (at the scale of 100 of meters) and subdaily variation in the glacier melt end-member tracer signature revealed no distinct effect on the mixing model results.

ACKNOWLEDGMENTS

This work is part of the project HydroGeM^3 and has been funded by the Austrian Academy of Sciences. We gratefully thank Nora Els, Tobias Horn, Felix Heinz, and the volunteers for their help during the field work. We also acknowledge the Center of Stable Isotope Analysis (CSI) at the Karlsruhe Institute of Technology (Institute of Meteorology and Climate Research—Atmospheric Environmental Research) for the water stable isotope analyses.

ORCID

Jan Schmieder http://orcid.org/0000-0003-1521-3984

REFERENCES

Ambach, W., Eisner, H., Elsässer, M., Löschhorn, U., Moser, H., Rauer, W., & Stichler, W. (1976). Deuterium, tritium and gross-beta-activity investigations on Alpine glaciers (Ötztal Alps). *Journal of Glaciology*, *17*, 383–400.

Baraer, M., McKenzie, J., Mark, B. G., Gordon, R., Bury, J., Condom, T., … Fortner, S. K. (2015). Contribution of groundwater to the outflow from ungauged glacierized catchments: A multi-site study in the tropical cordillera Blanca, Peru. *Hydrological Processes*, *29*, 2561–2581. https://doi.org/10.1002/hyp.10386

Baraer, M., McKenzie, J. M., Mark, B. G., Bury, J., & Knox, S. (2009). Characterizing contributions of glacier melt and groundwater during the dry season in a poorly gauged catchment of the Cordillera Blanca (Peru). *Advances in Geosciences*, *22*, 41–49. https://doi.org/10.5194/adgeo-22-41-2009

Barnett, T. P., Adam, J. C., & Lettenmaier, D. P. (2005). Potential impacts of a warming climate on water availability in snow-dominated regions. *Nature*, *438*, 303–309.

Beniston, M. (2012). Impacts of climatic change on water and associated economic activities in the Swiss Alps. *Journal of Hydrology*, *412–413*, 291–296. https://doi.org/10.1016/j.jhydrol.2010.06.046

Blaen, P. J., Hannah, D. M., Brown, L. E., & Milner, A. M. (2014). Water source dynamics of high Arctic river basins. *Hydrological Processes*, *28*, 3521–3538. https://doi.org/10.1002/hyp.9891

Buttle, J. M. (1994). Isotope hydrograph separations and rapid delivery of pre-event water from drainage basins. *Progress in Physical Geography*, *18*, 16–41. https://doi.org/10.1177/030913339401800102

Buttle, J. M. (2006). Isotope hydrograph separation of runoff sources. In *Encyclopedia of hydrological sciences*. John Wiley & Sons, Ltd.

Cable, J., Ogle, K., & Williams, D. (2011). Contribution of glacier meltwater to streamflow in the Wind River Range, Wyoming, inferred via a Bayesian mixing model applied to isotopic measurements. *Hydrological Processes*, *25*, 2228–2236. https://doi.org/10.1002/hyp.7982

CLC (2012). Corine Land Cover 2012 raster data. European Environment Agency. The European Topic Centre on Land Use and Spatial Information.

Collins, A. L., & Young, G. J. (1981). Meltwater hydrology and hydrochemistry in snow and ice-Covered Mountain catchments. *Hydrology Research*, *12*(4–5), 319–334.

Dahlke, H. E., Lyon, S. W., Jansson, P., Karlin, T., & Rosqvist, G. (2014). Isotopic investigation of runoff generation in a glacierized catchment in northern Sweden. *Hydrological Processes*, *28*, 1383–1398. https://doi.org/10.1002/hyp.9668

Dansgaard, W. (1964). Stable isotopes in precipitation. *Tellus*, *16*, 436–468. https://doi.org/10.1111/j.2153-3490.1964.tb00181.x

Drever, J. I. (1997). *The geochemistry of natural waters: Surface and groundwater environments*. Prentice Hall.

Dzikowski, M., & Jobard, S. (2012). Mixing law versus discharge and electrical conductivity relationships: Application to an alpine proglacial stream. *Hydrological Processes*, *26*, 2724–2732. https://doi.org/10.1002/hyp.8366

Engel, M., Penna, D., Bertoldi, G., Dell'Agnese, A., Soulsby, C., & Comiti, F. (2016). Identifying run-off contributions during melt-induced run-off events in a glacierized alpine catchment. *Hydrological Processes*, *30*, 343–364. https://doi.org/10.1002/hyp.10577

Fischer, B. M. C., Rinderer, M., Schneider, P., Ewen, T., & Seibert, J. (2015). Contributing sources to baseflow in pre-alpine headwaters using spatial snapshot sampling. *Hydrological Processes*, *29*, 5321–5336. https://doi.org/10.1002/hyp.10529

Fischer, B. M. C., Stähli, M., & Seibert, J. (2016). Pre-event water contributions to runoff events of different magnitude in pre-alpine headwaters. *Hydrology Research*, *48*(1), 28–47. https://doi.org/10.2166/nh.2016.176

Fountain, A. G. (1996). Effect of snow and firn hydrology on the physical and chemical characteristics of glacial runoff. *Hydrological Processes*, *10*, 509–521. https://doi.org/10.1002/(SICI)1099-1085(199604)10:4%3C509::AID-HYP389%3E3.0.CO;2-3

Frenierre, J. L., & Mark, B. G. (2014). A review of methods for estimating the contribution of glacial meltwater to total watershed discharge. *Progress in Physical Geography*, *38*, 173–200. https://doi.org/10.1177/0309133313516161

Frisbee, M. D., Phillips, F. M., Campbell, A. R., Liu, F., & Sanchez, S. A. (2011). Streamflow generation in a large, alpine watershed in the southern Rocky Mountains of Colorado: Is streamflow generation simply the aggregation of hillslope runoff responses? *Water Resources Research*, *47*. https://doi.org/10.1029/2010WR009391

Genereux, D. (1998). Quantifying uncertainty in tracer-based hydrograph separations. *Water Resources Research*, *34*, 915–919. https://doi.org/10.1029/98WR00010

Gleeson, T., & Manning, A. H. (2008). Regional groundwater flow in mountainous terrain: Three-dimensional simulations of topographic and hydrogeologic controls. *Water Resources Research*, *44*. https://doi.org/10.1029/2008WR006848

Hanzer, F., Förster, K., Nemec, J., & Strasser, U. (2017). Projected cryospheric and hydrological impacts of 21st century climate change in the Ötztal Alps (Austria) simulated using a physically based approach. *Hydrology and Earth System Sciences Discussions*, *2017*, 1–34. https://doi.org/10.5194/hess-2017-309

Hinton, M. J., Schiff, S. L., & English, M. C. (1994). Examining the contributions of glacial till water to storm runoff using two- and three-component hydrograph separations. *Water Resources Research*, *30*, 983–993. https://doi.org/10.1029/93WR03246

Hoeg, S., Uhlenbrook, S., & Leibundgut, C. (2000). Hydrograph separation in a mountainous catchment—Combining hydrochemical and isotopic tracers. *Hydrological Processes*, *14*, 1199–1216. https://doi.org/10.1002/(SICI)1099-1085(200005)14:7%3C1199::AID-HYP35%3E3.0.CO;2-K

Immerzeel, W. W., & Bierkens, M. F. P. (2012). Asia's water balance. *Nature Geoscience*, *5*, 841–842.

IPCC (2013). In T. F. Stocker, D. Qin, G.-K. Plattner, M. Tignor, S. K. Allen, J. Boschung, et al. (Eds.), *Climate change 2013: The physical science basis. Contribution of working group I to the fifth assessment report of the intergovernmental panel on climate change* (p. 1535). Cambridge, United Kingdom and New York, NY, USA: Cambridge University Press. https://doi.org/10.1017/CBO9781107415324

Jasechko, S., Kirchner, J. W., Welker, J. M., & McDonnell, J. J. (2016). Substantial proportion of global streamflow less than three months old. *Nature Geoscience*, *9*, 126–129. https://doi.org/10.1038/ngeo2636

Jeelani, G., Shah, R. A., Jacob, N., & Deshpande, R. D. (2017). Estimation of snow and glacier melt contribution to Liddar stream in a mountainous catchment, western Himalaya: An isotopic approach. *Isotopes in Environmental and Health Studies*, *53*(1), 18–35. https://doi.org/10.1080/10256016.2016.1186671

Kaser, G., Großhauser, M., & Marzeion, B. (2010). Contribution potential of glaciers to water availability in different climate regimes. *Proceedings of the National Academy of Sciences*, *107*, 20223–20227. https://doi.org/10.1073/pnas.1008162107

Kendall, C., & Doctor, D. H. (2003). Stable isotope applications in hydrologic studies. In H. D. Holland, & K. K. Turekian (Eds.), *Treatise on geochemistry* ()*Surface and ground water, weathering, and soils*. Oxford: Elsevier.

Klaus, J., & McDonnell, J. J. (2013). Hydrograph separation using stable isotopes: Review and evaluation. *Journal of Hydrology*, *505*, 47–64. https://doi.org/10.1016/j.jhydrol.2013.09.006

Kong, Y., & Pang, Z. (2012). Evaluating the sensitivity of glacier rivers to climate change based on hydrograph separation of discharge. *Journal of Hydrology*, *434-435*, 121–129. https://doi.org/10.1016/j.jhydrol.2012.02.029

Lang, H. (1986). Forecasting meltwater runoff from snow-covered areas and from glacier basins. In D. A. Kraijenhoff, & J. R. Moll (Eds.), *River flow modelling and forecasting*. Dordrecht: Springer Netherlands.

Lemke, P., Ren, J., Alley, R. B., Allison, I., Carrasco, J., Flato, G., … Zhang, T. (2007). Observations: Changes in snow, ice and frozen ground. In S. Solomon, D. Qin, M. Manning, Z. Chen, M. Marquis, K. B. Averyt, et al. (Eds.), *Climate change 2007: The physical science basis. Contribution of working group I to the fourth assessment report of the intergovernmental panel on climate change*. Cambridge, United Kingdom and New York, NY, USA: Cambridge University Press.

Liu, J., Han, X., Chen, X., Lin, H., & Wang, A. (2016). How well can the subsurface storage-discharge relation be interpreted and predicted using the geometric factors in headwater areas? *Hydrological Processes*, *30*, 4826–4840. https://doi.org/10.1002/hyp.10958

Liu, Y., Fan, N., An, S., Bai, X., Liu, F., Xu, Z., … Liu, S. (2008). Characteristics of water isotopes and hydrograph separation during the wet season in the Heishui River, China. *Journal of Hydrology*, *353*, 314–321. https://doi.org/10.1016/j.jhydrol.2008.02.017

Mark, B. G., McKenzie, J. M., & Gómez, J. (2005). Hydrochemical evaluation of changing glacier meltwater contribution to stream discharge: Callejon de Huaylas, Peru/evaluation hydrochimique de la contribution évolutive de la fonte glaciaire à l'écoulement fluvial: Callejon de Huaylas. *Pérou. Hydrological Sciences Journal*, *50*. https://doi.org/10.1623/hysj.2005.50.6.975

Marke, T., & Strasser, U. (2017). Continuous meteorological observations at station Latschbloder in 2015. In: In supplement to: Strasser, U., Marke, T., Braun, L., Escher-Vetter, H., Juen, I., Kuhn, M., . . . Kaser, G. (2018). The Rofental: a high Alpine research basin (1890 m - 3770 m a.s.l.) in the Ötztal Alps (Austria) with over 150 years of hydro-meteorological and glaciological observations. Special Issue: Hydrometeorological data from mountain and alpine research catchments; 04 Aug 2015–30 Sep 2017; Guest editors: J. Pomeroy, & D. Marks, Earth System Science Data, 21 pp, PANGAEA.

Maurya, A. S., Shah, M., Deshpande, R. D., Bhardwaj, R. M., Prasad, A., & Gupta, S. K. (2011). Hydrograph separation and precipitation source identification using stable water isotopes and conductivity: River Ganga at Himalayan foothills. *Hydrological Processes*, *25*, 1521–1530. https://doi.org/10.1002/hyp.7912

McDonnell, J. J., Bonell, M., Stewart, M. K., & Pearce, A. J. (1990). Deuterium variations in storm rainfall: Implications for stream hydrograph separation. *Water Resources Research*, *26*, 455–458. https://doi.org/10.1029/WR026i003p00455

Miller, J. D., Immerzeel, W. W., & Rees, G. (2012). Climate change impacts on glacier hydrology and river discharge in the Hindu Kush–Himalayas. *Mountain Research and Development*, *32*, 461–467. https://doi.org/10.1659/MRD-JOURNAL-D-12-00027.1

Miller, M. P., Buto, S. G., Susong, D. D., & Rumsey, C. A. (2016). The importance of base flow in sustaining surface water flow in the Upper Colorado River Basin. *Water Resources Research*, *52*, 3547–3562. https://doi.org/10.1002/2015WR017963

Moser, H., & Stichler, W. (1980). Environmental isotopes in ice and snow. In P. Fritz, & J. C. Fontes (Eds.), *Handbook of environmental isotope geochemistry*. New York: Elsevier.

Nolin, A. W., Phillippe, J., Jefferson, A., & Lewis, S. L. (2010). Present-day and future contributions of glacier runoff to summertime flows in a Pacific Northwest watershed: Implications for water resources. *Water Resources Research*, *46*. https://doi.org/10.1029/2009WR008968

Ogunkoya, O. O., & Jenkins, A. (1993). Analysis of storm hydrograph and flow pathways using a three-component hydrograph separation model. *Journal of Hydrology*, *142*, 71–88.

Ohlanders, N., Rodriguez, M., & McPhee, J. (2013). Stable water isotope variation in a Central Andean watershed dominated by glacier and snowmelt. *Hydrology and Earth System Sciences*, *17*, 1035–1050. https://doi.org/10.5194/hess-17-1035-2013

Penna, D., Engel, M., Bertoldi, G., & Comiti, F. (2017). Towards a tracer-based conceptualization of meltwater dynamics and streamflow response in a glacierized catchment. *Hydrology and Earth System Sciences*, *21*, 23–41. https://doi.org/10.5194/hess-21-23-2017

Penna, D., Engel, M., Mao, L., Dell'Agnese, A., Bertoldi, G., & Comiti, F. (2014). Tracer-based analysis of spatial and temporal variations of water sources in a glacierized catchment. *Hydrology and Earth System Sciences*, *18*, 5271–5288. https://doi.org/10.5194/hess-18-5271-2014

Pinder, G. F., & Jones, J. F. (1969). Determination of the ground-water component of peak discharge from the chemistry of total runoff. *Water Resources Research*, *5*, 438–445. https://doi.org/10.1029/WR005i002p00438

Prantl, H., Nicholson, L., Sailer, R., Hanzer, F., Juen, I., & Rastner, P. (2017). Glacier snowline determination from terrestrial laser scanning intensity data. *Geosciences*, *7*, 60.

Pu, T., He, Y., Zhu, G., Zhang, N., Du, J., & Wang, C. (2013). Characteristics of water stable isotopes and hydrograph separation in Baishui catchment during the wet season in Mt.Yulong region, south western China. *Hydrological Processes*, *27*, 3641–3648. https://doi.org/10.1002/hyp.9479

Racoviteanu, A. E., Armstrong, R., & Williams, M. W. (2013). Evaluation of an ice ablation model to estimate the contribution of melting glacier ice to annual discharge in the Nepal Himalaya. *Water Resources Research*, *49*, 5117–5133. https://doi.org/10.1002/wrcr.20370

Rixen, C., Teich, M., Lardelli, C., Gallati, D., Pohl, M., Pütz, M., & Bebi, P. (2011). Winter tourism and climate change in the Alps: An assessment

of resource consumption, snow reliability, and future snowmaking potential. *Mountain Research and Development*, *31*, 229–236. https://doi.org/10.1659/MRD-JOURNAL-D-10-00112.1

Rodhe, A. (1987). *The origin of streamwater traced by oxygen-18*. Uppsala University, Department of Physical Geography, Division of Hydrology.

Rodriguez, M., Ohlanders, N., Pellicciotti, F., Williams, M. W., & McPhee, J. (2016). Estimating runoff from a glacierized catchment using natural tracers in the semi-arid Andes cordillera. *Hydrological Processes*, *30*, 3609–3626. https://doi.org/10.1002/hyp.10973

Schaefli, B., Hingray, B., & Musy, A. (2007). Climate change and hydropower production in the Swiss Alps: Quantification of potential impacts and related modelling uncertainties. *Hydrology and Earth System Sciences*, *11*, 1191–1205. https://doi.org/10.5194/hess-11-1191-2007

Schaner, N., Voisin, N., Nijssen, B., & Lettenmaier, D. P. (2012). The contribution of glacier melt to streamflow. *Environmental Research Letters*, *7*, 034029.

Sklash, M. G. (1990). Environmental isotope studies of storm and snowmelt runoff generation. In M. G. Anderson, & T. P. Burt (Eds.), *Process studies in hillslope hydrology*. New York: John Wiley.

Staudinger, M., Stoelzle, M., Seeger, S., Seibert, J., Weiler, M., & Stahl, K. (2017). Catchment water storage variation with elevation. *Hydrological Processes*, *31*, 2000–2015. https://doi.org/10.1002/hyp.11158

Stewart, M. K., & McDonnell, J. J. (1991). Modeling base flow soil water residence times from deuterium concentrations. *Water Resources Research*, *27*, 2681–2693. https://doi.org/10.1029/91WR01569

Strasser, U., Marke, T., Braun, L., Escher-Vetter, H., Juen, I., Kuhn, M., … Kaser, G. (2018). The Rofental: A high Alpine research basin (1890–3770 m a.s.l.) in the Ötztal Alps (Austria) with over 150 years of hydrometeorological and glaciological observations. *Earth System Science Data*, *10*(1), 151–171. https://doi.org/10.5194/essd-10-151-2018

Uhlenbrook, S., & Hoeg, S. (2003). Quantifying uncertainties in tracer-based hydrograph separations: A case study for two-, three- and five-component hydrograph separations in a mountainous catchment. *Hydrological Processes*, *17*, 431–453. https://doi.org/10.1002/hyp.1134

Viviroli, D., Archer, D. R., Buytaert, W., Fowler, H. J., Greenwood, G. B., Hamlet, A. F., … Woods, R. (2011). Climate change and mountain water resources: Overview and recommendations for research, management and policy. *Hydrology and Earth System Sciences*, *15*, 471–504. https://doi.org/10.5194/hess-15-471-2011

WGMS. (2017). Fluctuations of Glaciers Database. World Glacier Monitoring Service, Zurich, Switzerland. https://doi.org/10.5904/wgms-fog-2017-10

Ward, R. C., & Robinson, M. (2000). *Principles of hydrology*. McGraw-Hill.

Weiler, M., McDonnell, J. J., Van Meerveld, H. J., & Uchida, T. (2005). Subsurface stormflow. In M. G. Anderson (Ed.), *Encyclopedia of hydrological sciences* (Vol. 3) (pp. 1719–1732). Hoboken, NJ, USA: John Wiley & Sons.

Williams, M. W., Wilson, A., Tshering, D., Thapa, P., & Kayastha, R. B. (2016). Using geochemical and isotopic chemistry to evaluate glacier melt contributions to the Chamkar Chhu (river), Bhutan. *Annals of Glaciology*, *57*, 339–348.

Wilson, A. M., Williams, M. W., Kayastha, R. B., & Racoviteanu, A. (2016). Use of a hydrologic mixing model to examine the roles of meltwater, precipitation and groundwater in the Langtang River basin, Nepal. *Annals of Glaciology*, *57*, 155–168. https://doi.org/10.3189/2016AoG71A067

Wu, J. -K., Ding, Y. -J., Yang, J. -H., Liu, S. -W., Chen, J. -Z., Zhou, J. -X., & Qin, X. (2016). Spatial variation of stable isotopes in different waters during melt season in the Laohugou Glacial Catchment, Shule River basin. *Journal of Mountain Science*, *13*, 1453–1463. https://doi.org/10.1007/s11629-014-3076-3

Yde, J. C., Knudsen, N. T., Steffensen, J. P., Carrivick, J. L., Hasholt, B., Ingeman-Nielsen, T., … Russell, A. J. (2016). Stable oxygen isotope variability in two contrasting glacier river catchments in Greenland. *Hydrology and Earth System Sciences*, *20*, 1197–1210. https://doi.org/10.5194/hess-20-1197-2016

Zhou, J., Wu, J., Liu, S., Zeng, G., Qin, J., Wang, X., & Zhao, Q. (2015). Hydrograph separation in the headwaters of the Shule River Basin: Combining water chemistry and stable isotopes. *Advances in Meteorology*, *2015*, 1–10. https://doi.org/10.1155/2015/830306

Zhou, S., Wang, Z., & Joswiak, D. R. (2014). From precipitation to runoff: Stable isotopic fractionation effect of glacier melting on a catchment scale. *Hydrological Processes*, *28*, 3341–3349. https://doi.org/10.1002/hyp.9911

SUPPORTING INFORMATION

Additional supporting information may be found online in the Supporting Information section at the end of the article.

How to cite this article: Schmieder J, Garvelmann J, Marke T, Strasser U. Spatio-temporal tracer variability in the glacier melt end-member — How does it affect hydrograph separation results?. *Hydrological Processes*. 2018;1–16. https://doi.org/10.1002/hyp.11628